

Microlensing in the Galactic Bulge: Effects of the Disk Behind the Bulge

Vibhat Nair and Jordi Miralda-Escudé¹

Department of Physics and Astronomy, University of Pennsylvania, Philadelphia, PA 19104

¹ Alfred P. Sloan Fellow

ABSTRACT

A large number of microlensing events have been observed in the direction of the Galactic bulge, with a measured optical depth in the range $2 - 3 \times 10^{-6}$. It has been shown that most of these events are due to bulge stars being lensed by other bulge stars or by foreground disk stars. Among the stars observed in the bulge fields, there should also be disk stars located behind the bulge; here, we consider their effect on the microlensing rates. The optical depth of background disk stars is much higher than that of typical bulge stars, reaching 10^{-5} at 6 kpc behind the bulge. Thus, although background disk stars are a very small fraction of the stars in Baade's window, we find that ~ 5 to 10% of the optical depth should be due to disk stars more than 3 kpc behind the bulge. This fraction is sensitive to the luminosity function of disk stars at large scale-height, to the magnitude cutoff of the survey, and to the amplification bias effect causing large numbers of "blended" events. We consider also the effect of a warp and flare in the disk at large distances behind the bulge; this could increase the optical depth from the background disk to $\sim 20\%$ of the total. Events on background disk stars should on average be longer than other events and could be distinguished also by measuring the proper motion or distance of the stars that have been microlensed. The number of these events could be an interesting probe to the structure and stellar population of the far-side of the Galactic disk.

Subject headings: Galaxy: structure - galaxies: Sagittarius dwarf - gravitational lensing

1. Introduction

Microlensing has emerged over the last few years as a new field in astrophysics capable of probing the nature of the dark matter, the structure of our Galaxy, and the mass

distribution of stars (see Paczyński 1996 for a review). So far, over 100 events have been detected in the bulge of our Galaxy, near Baade’s window (Alcock et al. 1997a), and over a dozen in the LMC (Udalski et al. 1993,1994; Alcock et al. 1997b). In both locations, the observed optical depth is larger than expected if we assume that the known stars are the only objects causing the microlensing events, although there remain substantial systematic errors in the theoretical calculations due to uncertainties in the spatial distribution of the stars, as well as statistical errors in the observational results.

The estimates of the microlensing optical depth to Baade’s window assumed first that most of the events would be caused by disk stars lensing sources in the bulge. After the first few events started to suggest a higher than expected value of the optical depth, it was pointed out by Kiraga & Paczyński (1994) that lenses in the bulge should actually be more important. For a source in the bulge, an event due to a lensing star in the bulge should typically have a much smaller Einstein radius, $\theta_E = [(4GM/c^2)(D_{ls}/D_l D_s)]^{1/2}$, compared to an event due to a disk lens, because the distance ratio D_{ls}/D_s is very small, given the small size of the bulge compared to its distance from us. However, the smaller Einstein radii are more than compensated for by the much larger abundance of bulge stars in the observed fields. The triaxiality of the bulge turns out to help as a way to increase the optical depth, due to the larger separation that is allowed between the lens and the source if the long axis is at a small angle relative to the line of sight. Assuming the maximum mass for the bulge that is consistent with dynamical measurements, an optical depth as high as $\sim 2 \times 10^{-6}$ is possible (Zhao, Spergel, & Rich 1995). This is still below the observed value, but consistent with it given the errorbars ($\tau = 2.4 \pm 0.5 \times 10^{-6}$ for all events and $\tau = 3.9^{+1.8}_{-1.2} \times 10^{-6}$ for clump giant events alone, in Alcock et al. 1997a; and $\tau = 3.3 \pm 1.2 \times 10^{-6}$ in Udalski et al. 1994).

In this paper, we shall analyze the contribution to the total optical depth of sources that are at larger distances than the bulge. These sources should generally belong to the disk of the Milky Way behind the bulge. Some of them could also be members of the recently discovered Sagittarius dwarf (Ibata et al. 1994), which was shown to extend to fields close to Baade’s window from a study of RR Lyrae variables (Alard 1996). Any such sources should have a much higher optical depth than the very numerous bulge sources, since they can be lensed by any bulge star with a large value of the distance ratio.

Mollerach & Roulet (1996) discussed the contribution to the optical depth from stars in the disk and estimated their event durations. In their models, they considered only sources within 3 kpc of the center of the Galaxy. In this paper we shall specifically address the contribution to the optical depth due to sources at larger distances. We also study the effect of a perturbation on the shape of the disk behind the bulge to the optical depth.

We find that in general, the events on background disk stars can only account for a small fraction of the total optical depth toward the bulge, and therefore cannot increase the total optical depth significantly above the predictions obtained by assuming that all sources are bulge stars (in practice, some sources are also foreground disk stars, and this reduces the mean optical depth). Nevertheless, the fraction of background disk events is still large enough to be detectable and may be of interest for studies of Galactic structure.

2. Models: Distribution of Lenses and Sources

Our purpose here is to illustrate the probable relative contribution of the background disk (i.e., the disk behind the bulge) to the optical depth determined in the microlensing experiments. We adopt the simple model for the mass distribution of the bulge derived from the best fit for triaxial models to the DIRBE maps of the bulge at $2.2\mu m$ (Model G2 of Dwek et al. 1995). This consists of a triaxial bulge with a total mass of $1.8 \times 10^{10} M_{\odot}$. The density distribution is as follows:

$$\begin{aligned} \rho_b &= 2.07 \exp\left(-\frac{w^2}{2}\right) M_{\odot} \text{ pc}^{-3}, \\ w^4 &= \left[\left(\frac{x'}{1580 \text{ pc}} \right)^2 + \left(\frac{y'}{620 \text{ pc}} \right)^2 \right]^2 + \left(\frac{z}{430 \text{ pc}} \right)^4, \end{aligned} \quad (1)$$

where x' and y' are in the plane of the disk, and the x' axis forms an angle of 20° relative to the x axis, which is the line from the Sun to the Galactic center (hereafter, GC). For the disk, we use the fit obtained by Gould, Bahcall, & Flynn (1997) to the HST star counts:

$$\rho_d = 0.055 \exp\left[\frac{(R_0 - R)}{3.5 \text{ kpc}}\right] \cdot \left[0.28 \cdot \exp\left[\frac{-|z|}{h_k}\right] + 0.72 \cdot \text{sech}^2\left[\frac{|z|}{(2 \cdot h_n)}\right] \right] M_{\odot} \text{ pc}^{-3}, \quad (2)$$

where R is the cylindrical radius from the GC, $R_0 = 8 \text{ kpc}$, and $h_k = 700 \text{ pc}$, $h_n = 175 \text{ pc}$ are the scale-heights of the thick and thin disks, respectively. The above model of the disk gives a value of $50 M_{\odot} / \text{pc}^2$ for the total star surface density of the disk at the solar radius, which is on the high side of present observational estimates of the density of luminous stars, but more consistent with dynamical estimates of the disk surface density (Gould 1990).

To calculate the mean optical depth for a population of sources, one needs to integrate the number of sources per unit solid angle at each distance with an apparent magnitude brighter than the limit of the microlensing experiment. In our models, knowledge of the luminosity function of the source stars is particularly important, given the wide

range of distances over which sources are located, and given our goal of comparing the contribution to the total optical depth of stars from different components of the Galaxy. We use two models for the luminosity function of stars, consisting of truncated power-law $\phi(L) dL \propto L^{-\beta-1} dL$, with three luminosity intervals of different β . Model 1 is based on the bulge luminosity function obtained by Holtzman et al. (1997), and corresponds to an old population of stars:

$$\begin{aligned} M_v > 4 & : \beta = -0.25 , \\ 2.75 < M_v < 4 & : \beta = -3.0 , \\ M_v < 2.75 & : \beta = -0.5 . \end{aligned} \tag{3}$$

We assume that both the bulge and the disk have this luminosity function in Model 1 . Model 2 has the same luminosity function for bulge stars, but for the disk we use the solar neighborhood luminosity function of Wielen et al. (1983), given by :

$$\begin{aligned} M_v > 4 & : \beta = -0.25 , \\ M_v < 4 & : \beta = -0.6 . \end{aligned} \tag{4}$$

Notice that the line of sight to Baade’s window reaches a large vertical height at the distance where most of the sources are located, so Model 1 is probably closer to reality because young stars are concentrated close to the mid-plane of the disk. Our results will be displayed for two apparent magnitude cutoffs, $m_t = 20$ and $m_t = 22$.

We also model the possibility that the background disk contains a large warp and flare. Evans et al. (1997) suggested that warping and flaring on our side of the disk might affect the optical depth to the Large Magellanic Cloud, and here we shall examine if warping and flaring on the opposite side of the disk could have an important effect on the microlensed stars in the bulge. Because of the large vertical gradient in the density of stars, the number of source stars at large distances behind the bulge might be altered appreciably by warping and flaring of the magnitude that is common in other galaxies (see Binney 1992 for a review). Thus, if the disk bends southward behind the bulge, the number of disk stars visible in Baade’s window (at Galactic latitude $b = -3.9^\circ$) could be greatly increased. We choose the following model to illustrate the possible effects:

$$R < R_0 : \quad h_k = 0.7 \text{ kpc} ,$$

$$\begin{aligned}
 h_n &= 0.175 \text{ kpc} , \\
 R > R_0 : \quad h_k &= 0.7 \left(\frac{R-R_0}{R_0} \right)^2 \text{ kpc} , \\
 h_n &= 0.175 \left(\frac{R-R_0}{R_0} \right)^2 \text{ kpc} .
 \end{aligned} \tag{5}$$

The mid-plane of the disk is assumed to be at a height z_w given by

$$\begin{aligned}
 R < R_0 &: \quad z_w = 0 \text{ kpc}, \\
 R > R_0 &: \quad z_w = 1.0 \left(\frac{R-R_0}{R_0} \right)^2 \cos(\phi + 70^\circ) \text{ kpc} .
 \end{aligned} \tag{6}$$

In the flared and warped disk model we use these values for h_k and h_n in equation 2, and replace z by $z - z_w$.

The above model for the warp and flare of the disk is consistent with observations of the distribution of neutral hydrogen in the disk (Diplas & Savage 1990). The observations constrain the angle of the line of nodes with respect to the Sun-GC line to be small, but with an error of $\sim 10^\circ$, and a larger uncertainty in the far side of the disk due to the scarcity of observations in that region. Of course, the larger this angle, the more important the effect of the warp will be for the microlensing event rates from background disk sources. Here we choose this angle to be 20° . The line of nodes does not necessarily have to be at a constant angle, since the warp could be twisted (i.e., the shape of the disk may in general have some two-dimensional Gaussian curvature).

3. Tidal Perturbation of the Disk by the Sagittarius dwarf

One of the reasons why the disk could be warped is the gravitational tidal perturbation caused by a satellite galaxy. In addition to the above simple model for a warp and flare, we shall examine another model based on the distortion of the disk induced by the gravitational perturbation of the Sagittarius dwarf.

The Sagittarius dwarf, discovered by Ibata et al. (1994, 1995) in a spectroscopic study of the Galactic bulge, is the closest galaxy to the Milky Way. It is located ~ 15 kpc behind the bulge, centered approximately at $l = 5.6^\circ$, $b = -14^\circ$, and is extended perpendicular to the Galactic plane over at least 20° in the sky. Its projected shape is elongated with an axis ratio 3 : 1. Its radial velocity is 140 km s^{-1} , moving away from us, and the proper motion indicates that it is moving upwards toward the disk, although the component parallel to

the disk is not yet accurately measured (Ibata et al. 1997). The luminosity of the galaxy is $\sim 10^7 L_\odot$.

The tidal perturbation that the Sagittarius dwarf will exert on the disk depends of course on its past trajectory and on its mass, which is highly uncertain depending on the mass of the dark matter halo surrounding the visible stars. We now describe a simple model that we use to obtain an estimate of the maximum plausible effect of this tidal perturbation.

The past trajectory of the Sagittarius dwarf is calculated as if it was a point mass moving in the Galactic potential, starting from its present position and velocity. Table 5 gives the present velocity of the dwarf in cylindrical coordinates, relative to the Sun and to the GC, denoted by subscripts h (for heliocentric) and G respectively. We fix the present position of the dwarf to be $l = 5.6^\circ$, $b = -14^\circ$, $r_h = 24$ kpc, r_h being the distance of the dwarf from the Sun (Ibata et al. 1997). We take $v_{h,r} = 140$ km s $^{-1}$ and $v_{h,z} = 150$ km s $^{-1}$. The z velocity is chosen to be small within the range consistent with the available error bars (Ibata et al. 1997), in order to maximize the perturbation on the disk. For $v_{G,\phi}$, the transverse velocity of the dwarf parallel to the disk, we use a range of values between 50 km s $^{-1}$ and 250 km s $^{-1}$. Because the major axis of the dwarf is almost perpendicular to the disk, and the tidal elongation of the structure of the dwarf is most likely to occur along its orbit, $v_{G,\phi}$ (which as yet is observationally undetermined) is likely to be small. However, the present shape of the dwarf should also depend on its internal kinematic structure, and a larger azimuthal velocity has not been ruled out. Note that we have assumed that the velocity of the dwarf is in the same sense as that of the rotation of the disk, which again maximizes the perturbation on the disk.

For the Galactic potential, we use a three-component model with an exponential disk, a bulge and a halo. We model the bulge as a $1.8 \times 10^{10} M_\odot$ point mass (sufficient for our purpose since we only need to evaluate the force at large distances from the GC), a halo with an 8 kpc core and velocity dispersion of 155 km s $^{-1}$, and an exponential disk with scale-length $R_d = 3.5$ kpc and central surface density $\Sigma_0 = 680 M_\odot/\text{pc}^2$. The circular velocity profile obtained for this model is nearly flat from $R = 5$ kpc to $R = 50$ kpc at a value of 200 km s $^{-1}$.

The trajectories obtained for the different choices of $v_{G,\phi}$ are shown in Figures 1 and 2.

Given the trajectory of the dwarf, we then consider stars moving initially in the plane of the disk on circular orbits, and calculate the perturbation of their trajectories due to the tidal acceleration caused by the gravity of the Sagittarius dwarf, equal to the gravitational acceleration acting on the star minus the acceleration acting on the GC. We use the approximation that the gravitational force of the Galaxy is always directed to the center,

even though the star will move out of the plane of the disk as a result of the tidal force. This is a reasonable approximation because, locally, the entire disk should be distorted by the perturbing tidal force in the same way, so the star should remain in the midplane of the perturbed disk. On a large scale, the disk will of course no longer be confined to a plane, but including the potential of the distorted disk would require a full N-body calculation. We have instead used this simple approximation, which should be valid at large radius, where the stars do not complete many orbits over the duration of the tidal perturbation.

For the mass density profile of the dwarf, we assume a spherical singular isothermal halo with a cutoff at 10 kpc, and a total mass of $5 \times 10^9 M_\odot$. Thus, the mass within 2 kpc is $10^9 M_\odot$, in agreement with the model of Ibata et al. (1997) reproducing the observed stellar velocity dispersion. The extent of the dwarf halo (and therefore its mass) is generally estimated to be smaller if the dwarf has already completed several orbits around the Galaxy, because it should have been tidally disrupted (e.g., Velázquez & White 1995, Ibata et al. 1997). However, the dwarf could be on its first orbit if its direction of motion was not the same as the direction of its elongation, or if its orbit had been recently perturbed. For example, the Sagittarius dwarf might originally have been a distant satellite of the Magellanic Clouds, and could be on its first orbit since being tidally pulled from that system. In a recent paper, Zhao (1998a) describes such a collision scenario of the Sagittarius dwarf with the Magellanic clouds. While his model assumes the mass of the Sagittarius dwarf to be much smaller than that of the Magellanic clouds, the orbit of the dwarf is not constrained well enough currently for this to be the only possibility. In this paper, we seek to estimate the maximum possible effect that the Sagittarius dwarf might have on the optical depth towards Baade’s window. Towards this end we have chosen the mass of the dwarf to be considerably larger than the estimates derived from the current models of its orbit.

The integration of the orbits of stars in the disk was started at 3×10^8 years into the past; all stars are initialized on circular orbits in the disk plane. The final vertical positions of the stars along our line of sight through Baade’s window are plotted in Figure 3, for the three values of the present azimuthal velocity of the Sagittarius dwarf. The vertical displacement in the GC vanishes by definition, since the tidal force acting on every star is defined relative to the GC. We have also fixed the displacement to zero at the position of the Sun, by assuming that the plane of the Galaxy is redefined to contain the Sun-GC line.

The effect of the perturbation can be separated into four regions along the line of sight: (1) The foreground disk stars are displaced southward relative to the Sun-GC line. (2) Immediately behind the bulge, stars are displaced northward due to the greater force that has acted on the GC compared to the Sun or the stars in this location. (3) Stars

lying between ~ 5 and 15 kpc behind the bulge are again displaced southward when the azimuthal velocity of the Sagittarius dwarf is high, owing to the more recent force acting on these stars as the Sagittarius dwarf approaches them from the South, following their orbital azimuthal motion. This part of the background disk can be pulled down by as much as 250 pc, a distance greater than the thin disk scale-height of 175 pc. (4) At distances greater than ~ 25 kpc, stars are displaced northward by several scale-heights; this is mainly due to the tidal force that has pulled down the GC relative to the Sun.

To summarize, the results in Figure 3 show that the only region where the number of sources could be increased substantially by this disk perturbation is in the 5 or 10 kpc immediately preceding the Sagittarius dwarf, along the line of sight near Baade’s window.

4. Results for the Optical Depth: Models with Unperturbed Disk

The optical depth of a source as a function of its distance from the Sun along Baade’s window (specifically, along the Galactic coordinates $\ell = 1^\circ$ and $b = -3.9^\circ$) is shown in Figure 4 for our unperturbed disk model (the difference of this curve in the models with a perturbed disk is negligible). The optical depth increases dramatically at the distance of the bulge, since most of the lenses are located there. Behind the bulge the optical depth continues to grow owing to the increasing distance ratio with the bulge lenses. Because the number of lenses beyond the bulge is very small, the optical depth approaches a constant value of almost 2×10^{-5} at very large distances, nearly ten times greater than the mean optical depth determined observationally. Thus, even a small fraction of background disk stars among the observed sources could have significant effects on the observed microlensing events. A similar phenomenon might take place for microlensing on the Large Magellanic Cloud (LMC), if some of the observed stars are in star-forming regions along tidal debris of the Magellanic clouds located far behind the LMC (Zhao 1998b).

Tables 1 to 4 give the contribution to the number of sources and the optical depth from various components of our Galaxy. The quantity f_i is the fraction of all the sources brighter than the apparent magnitude threshold, m , which belong to each component i . The mean optical depth τ_i of each component is

$$\tau_i = \frac{\int \rho_i(D_s, m) \tau(D_s) D_s^2 dD_s}{\int \rho_i(D_s, m) D_s^2 dD_s}, \quad (7)$$

where $\rho_i(D_s, m)$ is the density of sources of component i at distance D_s above the magnitude threshold m , and $\tau(D_s)$ is the optical depth for a source at distance D_s .

Thus, $\sum \tau_i f_i = \tau$, where τ is the mean optical depth for all sources above the

magnitude cutoff. We shall be ignoring dust obscuration here; in practice, most of the dust in the line of sight to the bulge fields searched for microlensing is close to the Sun, so practically all the sources have the same obscuration, and the effect of dust is then to simply change the value of the apparent magnitude cutoff.

For both models of the luminosity function, the contribution of the background disk to the mean optical depth, usually neglected, is significant. For the unperturbed disk (see Tables 1 through 4), the background disk contribution is at least $\sim 14\%$, and could be as high as $\sim 27\%$ in Model 2 for the luminosity function. Notice, though, that a lot of this contribution is due to sources close to the center, where the disk should probably be truncated due to the presence of the bar: the optical depth contribution from background disk stars located more than 3 kpc behind the GC is only $\sim 6\%$ in Model 1. These contributions depend sensitively on the luminosity function of the source stars and on the apparent magnitude cutoff of the survey, as we see in the Tables.

In Model 1, the disk has a luminosity function appropriate for old stars, implying that the number of stars declines abruptly at luminosities greater than the main-sequence turnoff (eq. 3). This results in a rapid decrease of sources at distances further than the point where the main-sequence turnoff coincides with the magnitude limit of the microlensing survey. In the absence of extinction, this distance is 16 (28) kpc for a threshold $m_t = 20$ (22). This is the reason why the contribution from stars in the background disk increases as fainter sources can be observed (or in regions of lower extinction). Model 2 also predicts a greater fraction of the optical depth from distant disk stars, owing to the greater abundance of luminous stars acting as microlensing sources when a young population is assumed to be present.

The fraction of the optical depth contributed by sources at each distance D_s is shown in Figure 5, for the two luminosity function models for $m_t = 20$. The average duration of events on background disk sources is larger than for events on bulge sources (this will be discussed in detail toward the end of this section). Because of the longer average duration of events, the contribution to the rate of events by background disk sources is smaller than the contribution to the optical depth.

The results presented in Tables 1-4 and Figure 5 do not take into account the effect of magnification bias. The fraction of microlensed stars located at each distance is valid for sources above a fixed magnitude cutoff when there is no lensing amplification. In practice, many of the microlensing events occur on sources which are fainter than the magnitude limit of the survey, but are brought above the limit during the microlensing event. Often these sources will be blended with a brighter star, so it is not always possible to know what the magnitude of the unlensed star is. This blending effect should result in an increased

contribution by distant sources to the observed microlensing events, because the magnitude threshold is effectively changed to fainter levels. On the other hand, extinction will raise the magnitude threshold. In order to compare model predictions of the distribution of source distances with observations, it will be necessary to securely identify and to measure the unlensed flux of every star that has been microlensed. Spectroscopy is probably difficult in these faint stars in crowded fields; but possibly, some clear photometric indicator that can select stars in the background disk may be identified (for example, stars located between the giant branch and main sequence of the bulge stars, after correction for extinction, would probably be giants in the background disk), which could make it possible to measure the enhancement of the fraction of distant sources among the microlensed stars compared to a random sample of sources in the bulge fields. Another way to distinguish background disk stars from bulge stars are proper motions. Background disk stars should always be moving along the plane in the direction of decreasing longitude, with $\mu \sim (80\text{kpc})/D_s \text{mas/yr}$, where D_s is the distance to the star from the sun. Thus for a typical disk source behind the bulge at $\sim 12\text{ kpc}$, $\mu \sim 6\text{mas/yr}$. Although bulge stars can also have similar proper motions, the two populations could be statistically separated.

The inclusion of source stars in the disk for the computation of the total microlensing optical depth in Baade’s window does not change the result by a large factor, compared to models where only bulge sources are included. Stars in the background disk certainly increase the total optical depth, by $\sim 10\%$ depending on the model; however, foreground disk stars also need to be included as sources, resulting in a decrease of the optical depth that tends to cancel the effect of the background disk in most cases. This is the reason why the total optical depth is generally not very different from the bulge optical depth.

If microlensing events could be detected along lines of sight at lower Galactic latitude compared to Baade’s window, a much larger contribution to the total optical depth from sources in the background disk should be expected. As an example, Table 5 gives the contributions of various components to the total optical depth for the line of sight at $l = 1^\circ, b = -1^\circ$. In this case, stars in the disk beyond 3 kpc from the bulge account for 5% of all sources and 20% of the optical depth, compared to 1.6% and 5%, respectively, in Baade’s window. Observations at these low Galactic latitudes would only be feasible for a microlensing survey in the infrared, due to the high obscuration.

In general, events on background disk stars should be of longer duration than events on bulge stars, owing to two reasons. First, the Einstein radius is larger for a source in the disk, due to the larger distance ratio D_{ls}/D_s when the source is in the background disk, since most of the lenses are in the bulge. Second, the relative proper motion of the lens and the source is smaller for a disk source. To see this, consider the proper motions of the

lens and the source relative to the Galactic center. The proper motion of the lens always has the same distribution, but the proper motion of the source relative to the Galactic center is generally smaller for a background disk source because the effect of the velocities of the source and the Sun have opposite sign (for example, the proper motion relative to the Galactic center is zero for a source at the same distance behind the Galactic center as the Sun). The velocity dispersion of disk sources is also small compared to that of bulge sources. Therefore, among the longest events, the fraction of microlensed stars belonging to the background disk should be higher than for shorter events.

Figure 6 shows the distribution of event durations for sources at three different distances, as indicated in the figure. We assume that all the lenses have a mass of $1M_{\odot}$, for the purpose of illustration. We also consider only bulge lenses, with a spherically symmetric Gaussian distribution of velocities with dispersion equal to 150 km s^{-1} . The disk sources are moving with constant circular velocity $V_c = 200 \text{ km s}^{-1}$, and dispersion of 50 km s^{-1} . The calculation was made using Monte-Carlo simulations of 10^6 events for each source distance. Sources at 16 kpc have longer durations by as much as a factor 2 compared to sources at 10 kpc (a typical distance for a bulge source). Introducing a distribution for the mass of the lens will have the effect of broadening the curves shown in Figure 6. This suggests that a long event duration may not be a very good discriminant for background disk events, given the large dispersion in lens mass. At the same time the contribution of background disk sources to the number of microlensing events should not be very different from the contribution to the total optical depth computed in this paper, since the difference in the mean event duration is not very large.

5. Effect of a Perturbed Disk on the Optical Depth

The flared and warped model of the disk, introduced in §2, increases the number of sources at large distances behind the bulge by reducing the distance from Baade’s window to the plane of the perturbed disk, and by increasing the disk scale-height. Thus, in Model 1, the disk perturbation increases the fraction of sources at distances greater than 15 kpc by a factor of 1.5, from 0.2% to 0.3%, at $m_t = 20$. The fraction of fainter sources ($m_t = 22$) is increased by a factor of 2, to 1.3%, and for Model 2 of the luminosity function this fraction can be as high as 2.3%.

The flared and warped disk results in a similar increase of the optical depth due to background disk stars. For example, in Model 2 and for $m_t = 22$, the fraction of the optical depth from sources at distances greater than 15 kpc is increased from 5% to 12%. Figure 5 also shows the distance distribution of the microlensed stars for the perturbed disk model,

with Model 1 of the luminosity function.

These results show how the measurement of the distance distribution of the microlensed stars in the bulge fields (which, as mentioned above, could be estimated from photometry and proper motions) could be used to constrain the structure of the disk in the far side of the Galaxy. These constraints would require an accurate knowledge of the luminosity function of the background disk stars, to which our results are also very sensitive to.

6. Effect of the Sagittarius Dwarf

Results are also given in Tables 1 and 2 for the models where the perturbation of the disk is caused by the tidal force of the Sagittarius dwarf. The effect of this perturbation is generally very small. In fact, in many cases the optical depth contributed by the background disk is decreased, owing to the northward displacement of the background disk sources close to the bulge (see Figure 3). The perturbation by the Sagittarius dwarf also causes the foreground disk (in front of the bulge) to be bent southward. This has two opposite effects on the total optical depth: the number of disk lenses increases, so the optical depth of every component also increases; but the number of foreground disk sources is also increased relative to the bulge sources, and this reduces the mean optical depth.

However, the effect of the stars in the Sagittarius dwarf acting as *sources* for microlensing may be important. A simple estimate of their effect compared to background disk stars at a similar distance may be obtained as follows. The Sagittarius dwarf has a total luminosity of $10^7 L_\odot$, spread over ~ 200 square degrees of the sky (Ibata et al. 1997), or 30 kpc^2 . This yields a surface luminosity density of $0.3 L_\odot \text{ pc}^{-2}$. For the disk, the surface luminosity density at the solar orbit is $15 L_\odot \text{ pc}^{-2}$; the Sagittarius dwarf is about two scale-lengths further away from the center than the Sun, so the disk surface luminosity density at that distance is $\sim 1.8 L_\odot \text{ pc}^{-2}$. Along Baade’s window and at the distance of the Sagittarius dwarf, the height below the plane is 1.6 kpc. Therefore, the luminosity density at this position integrated over a scale-length, for our model in equation (2), is reduced by a factor

$$0.72e^{-9.2}(3.5 \text{ kpc}/0.175 \text{ kpc})/2 + 0.28e^{-2.3}(3.5 \text{ kpc}/0.7 \text{ kpc})/2 , \quad (8)$$

to $0.15 L_\odot \text{ pc}^2$. According to this, the Sagittarius dwarf stars are two times as abundant as background disk stars at the same distance range, although disk stars slightly closer to us (at distances of one to three scale-lengths behind the bulge) should dominate over the Sagittarius dwarf stars. Microlensing events on stars in the background disk and the Sagittarius dwarf can be distinguished if proper motions are available. Proper motions have been measured in some stars in Sagittarius dwarf, although with relatively poor accuracy

(Ibata et al. 1997).

7. Conclusions

This paper has discussed the contribution of background disk sources to the total optical depth of microlensing events observed in Baade’s window. This contribution is appreciable and needs to be taken into account in comparisons between theoretical predictions and the observations. About 15% of the optical depth in Baade’s window is due to background disk stars; about half of this is contributed by stars at a distance greater than 3 kpc behind the bulge. This fraction is sensitive to the luminosity function of the source stars and the apparent magnitude limit of the microlensing survey (and therefore, to the “blending effects”). The possibility that the far-side of the disk is strongly warped and flared has also been considered, and we showed that this could significantly increase the number of background disk stars in Baade’s window. Our results may be taken as upper limits on the contribution of disk perturbations to the optical depth, since we have chosen the most favorable parameters in our models (e.g., the angle of the line of nodes for the warp and flare model was chosen to be 20° , and a large mass of the Sagittarius dwarf was assumed).

Future microlensing surveys towards the bulge could provide an interesting probe to the structure and the stellar population of the Galactic disk behind the bulge. We have focused in this paper on predicting the contribution to the microlensing event rate on Baade’s window, at a Galactic latitude $b \simeq -4^\circ$, because the present surveys are being done near this area of low extinction. However, in lines of sight closer to the Galactic plane, the density of disk stars should decrease more slowly with distance, and the contribution of background disk stars should therefore be much higher; an example has been presented in Table 5. Extinction should of course be very high at lower Galactic latitude, so microlensing surveys in this area would probably need to be carried out in the infrared. This may become more feasible as the size of CCD cameras sensitive in the infrared increases.

We would like to thank the referee, Dr. HongSheng Zhao, for his comments and suggestions that have improved the content and the presentation of this paper.

REFERENCES

- Alard, C. 1996, ApJ, 458, L17
- Alcock et al. 1997a, ApJ, 479, 119
- Alcock et al. 1997b, Bull. of Amer. Astr. Soc., 191, #83.01
- Binney, J. 1992, ARA&A, 30, 51
- Diplas, A. & Savage, B. D., 1990, ApJ, 377, 126
- Dwek, E. et al. 1995, ApJ, 445, 716
- Evans et al. Nature, submitted (1997)
- Gould, A., Bahcall, J. N., & Flynn, C. 1997, ApJ, 482, 913
- Gould, A., 1990, MNRAS, 244, 25
- Ibata, R., & Gilmore, G. 1994, Nature, 370, 194
- Ibata, R., & Gilmore, G. 1995, MNRAS, 275, L23
- Ibata, R., et al. 1997, Astronomical journal, 113, 634
- Holtzman, J. A., Watson, A. M., Baum, W. A., Grillmair, C. J., Groth, E. J., Light, R. M., Lynds, R., & O’Neil, E. J., Jr. 1997, AJ, in press.
- Kiraga, M., & Paczyński, B. 1994, ApJ, 430, L101
- Mollerach, S., & Roulet, E. 1996, ApJ, 458, L9
- Paczynski B. 1996, ARA & A, Vol. 34, 419
- Udalski et al. 1993, Acta Astronomica, 43, 289
- Udalski et al. 1994, Acta Astronomica, 44, 165
- Velázquez H., & White S. 1995, MNRAS, 275, L23
- Wielen, R., Jahreiss, H., & Kruger, R. 1983, in *Nearby Stars and the Stellar Luminosity Function*, IAU Coll. 76, eds. A. G. Davis Phillip & A. R. Upgren (Shenectady: L. Davis Press), p. 163
- Zhao, H. S. 1998a, ApJ, 500, L149

Zhao, H. S. 1998b, MNRAS, 294, 139

Zhao, H. S., Spergel, D. N., & Rich, M. 1995, ApJ ,440, L13

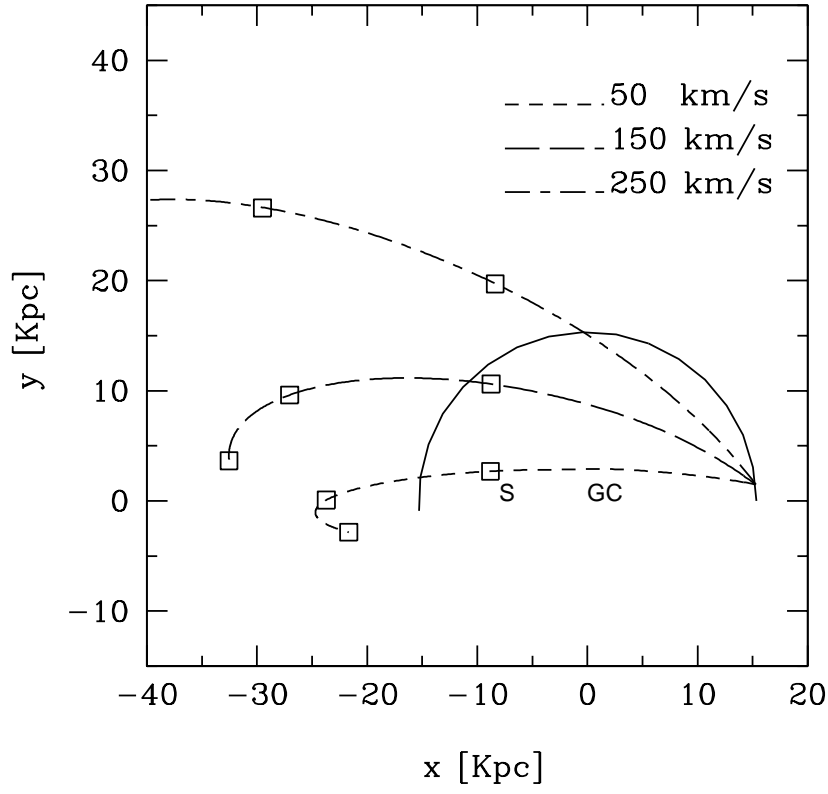


Fig. 1.— Orbit of the Sagittarius dwarf projected on the x-y plane, for the three cases of $v_{G,\phi}$ indicated in the figure. The positions at 10^8 year intervals are marked by squares. The circle has been shown to indicate the unperturbed orbit of a star at a radius of 15 kpc.

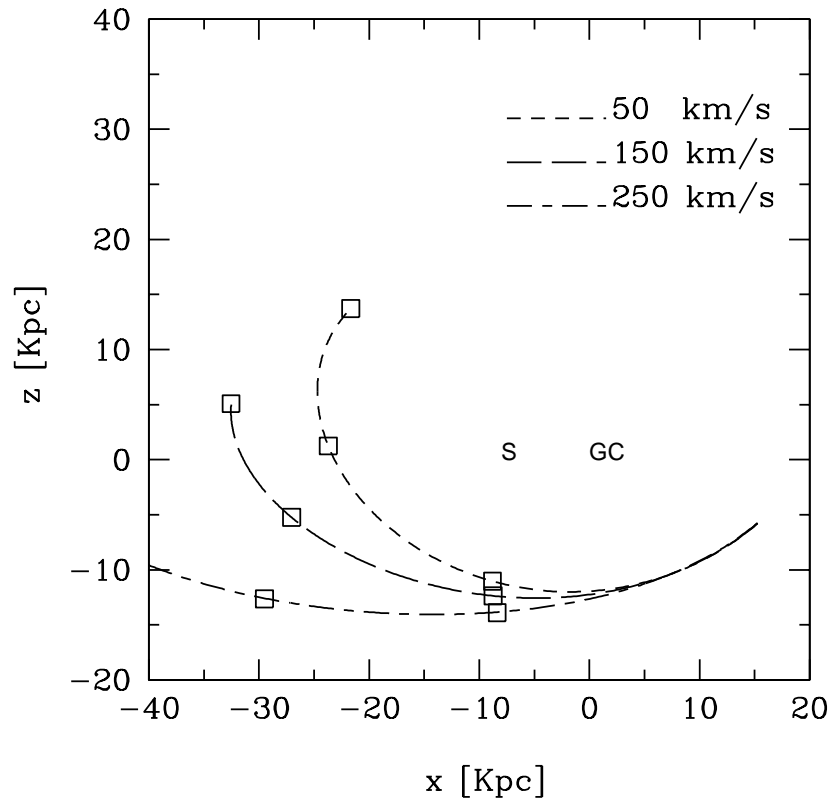


Fig. 2.— Orbit of the Sagittarius dwarf projected on the x - z plane, for the three cases of $v_{G,\phi}$ indicated in the figure. The positions at 10^8 year intervals are marked by squares.

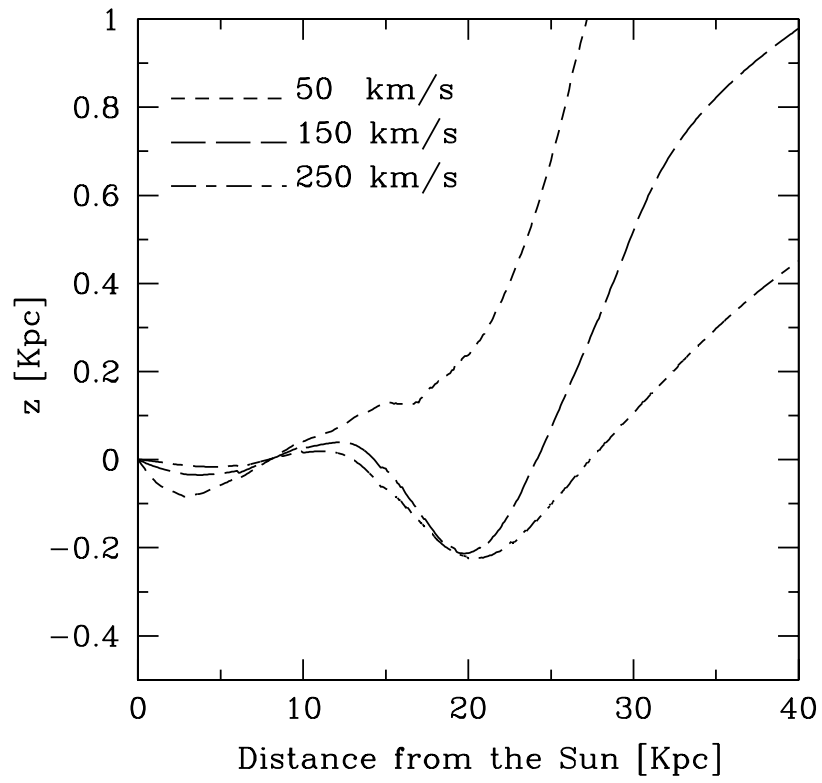


Fig. 3.— Final height of the stars with respect to the sun-GC line, for the three cases of $v_{G,\phi}$ indicated in the figure.

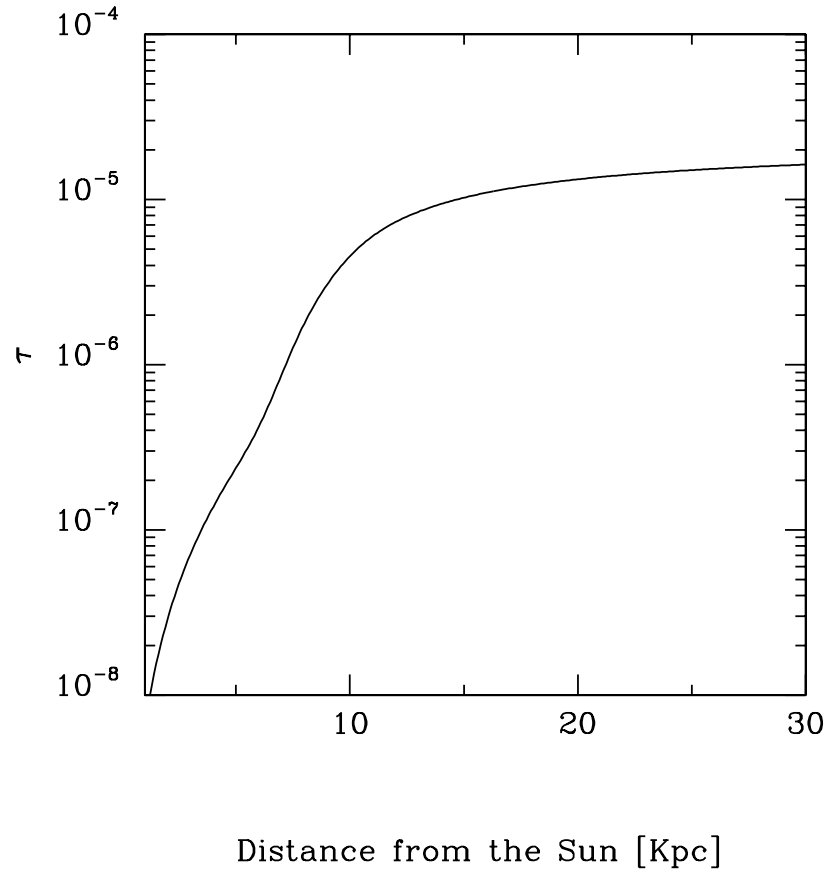


Fig. 4.— The optical depth τ , as a function of source distance along our line of sight through Baade’s window. Only the unperturbed case is shown. The difference from the unperturbed case is negligible for other cases.

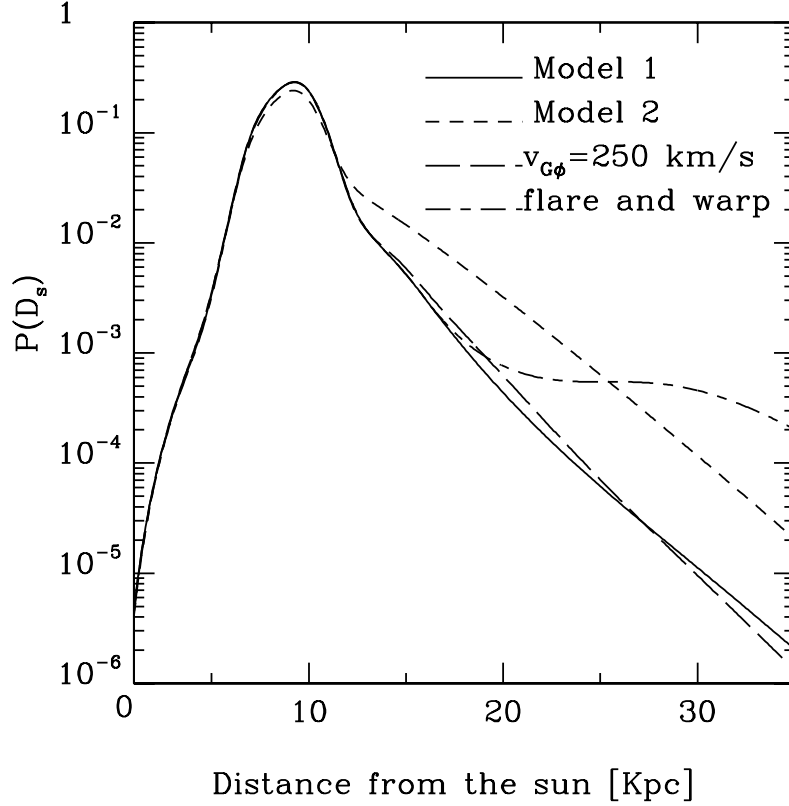


Fig. 5.— $P(D_s) \cdot dD_s$ is the fraction of the optical depth contributed by sources at distances between D_s and $D_s + dD_s$ from the sun. The solid, long dashed and dot dashed line correspond to an unperturbed disk, disk perturbed by the Sagittarius dwarf galaxy with $v_{G,\phi} = 250 \text{ km s}^{-1}$, and a warped and flared model of the disk, respectively. For all three we assume Model 1 for the luminosity function and a magnitude cutoff of 20. The short-dashed line corresponds to an unperturbed disk with Model 2 for the luminosity function and a magnitude cutoff of 20.

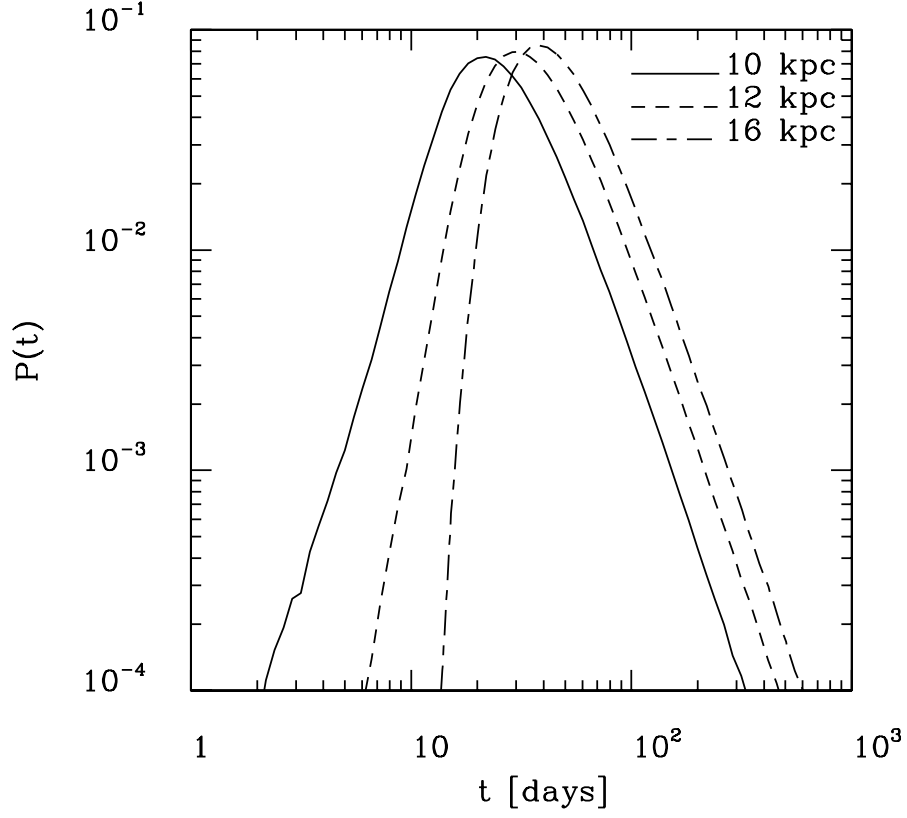


Fig. 6.— $P(t) \cdot dt$ is the probability, for a fixed source distance, that a lensing event on a source has an event duration between t and $t + dt$. Three cases, a bulge source at 10 kpc, and disk sources at 12 and 16 kpc have been shown. In all three cases, the lens is in the bulge and has a mass of $1M_{\odot}$. Isotropic, Gaussian velocity distributions were assumed for both the bulge and the disk, with dispersion equal to 150 km s^{-1} and 50 km s^{-1} , respectively.

Table 1. Model 1, $m_t = 20$

Model	Component (i)	$10^6 \tau_i$	$100 f_i$	$10^8 \left(\frac{\tau_i \cdot f_i}{\tau} \right)$
Unperturbed	Disk foreground	0.58	10.8	2.9
Unperturbed	Disk background	4.51	6.8	14.1
Unperturbed	Disk Total	2.085	17.5	16.9
Unperturbed	Disk > 15 kpc	11.52	0.2	1.0
Unperturbed	Disk > 11 kpc	8.13	1.6	5.1
Unperturbed	Bulge	2.18	82.5	83.1
Unperturbed	Total	2.16	100.0	100.0
Flare and warp	Disk foreground	0.58	10.8	2.9
Flare and warp	Disk background	4.68	6.8	14.7
Flare and warp	Disk Total	2.16	17.6	17.5
Flare and warp	Disk > 15 kpc	12.88	0.3	1.8
Flare and warp	Disk > 11 kpc	8.58	1.7	6.8
Flare and warp	Bulge	2.18	82.30	82.5
Flare and warp	Total	2.18	100.0	100.0
SD, $v_{G,\phi} = 50$	Disk foreground	0.60	12.1	3.3
SD, $v_{G,\phi} = 50$	Disk background	4.50	6.1	12.3
SD, $v_{G,\phi} = 50$	Disk Total	1.90	18.2	15.6
SD, $v_{G,\phi} = 50$	Disk > 15 kpc	11.57	0.15	0.8
SD, $v_{G,\phi} = 50$	Disk > 11 kpc	8.21	1.3	5.0
SD, $v_{G,\phi} = 50$	Bulge	2.29	81.8	84.4
SD, $v_{G,\phi} = 50$	Disk+Bulge	2.22	100.0	100.0
SD, $v_{G,\phi} = 150$	Disk foreground	0.59	11.5	3.1
SD, $v_{G,\phi} = 150$	Disk background	4.60	6.4	13.4
SD, $v_{G,\phi} = 150$	Disk Total	2.02	17.9	16.5
SD, $v_{G,\phi} = 150$	Disk > 15 kpc	11.65	0.2	1.2
SD, $v_{G,\phi} = 150$	Disk > 11 kpc	8.34	1.5	5.9
SD, $v_{G,\phi} = 150$	Bulge	2.23	82.1	83.5
SD, $v_{G,\phi} = 150$	Disk+Bulge	2.19	100.0	100.0
SD, $v_{G,\phi} = 250$	Disk foreground	0.58	11.2	3.0
SD, $v_{G,\phi} = 250$	Disk background	4.62	6.6	13.95
SD, $v_{G,\phi} = 250$	Disk Total	2.08	17.8	16.9
SD, $v_{G,\phi} = 250$	Disk > 15 kpc	11.62	0.2	1.3
SD, $v_{G,\phi} = 250$	Disk > 11 kpc	8.3	1.6	6.3
SD, $v_{G,\phi} = 250$	Bulge	2.20	82.2	83.1
SD, $v_{G,\phi} = 250$	Disk+Bulge	2.18	100.0	100.0

Table 2. Model 1, $m_t = 22$

Model	Component	$10^6 \tau_i$	$100 f_i$	$10^8 \left(\frac{\tau_i \cdot f_i}{\tau} \right)$
Unperturbed	Disk foreground	0.62	9.2	2.4
Unperturbed	Disk background	5.24	8.3	18.0
Unperturbed	Disk Total	2.81	17.5	20.3
Unperturbed	Disk > 15 kpc	11.9	0.66	3.3
Unperturbed	Disk > 11 kpc	8.81	2.8	10.2
Unperturbed	Bulge	2.33	82.5	79.7
Unperturbed	Total	2.41	100.0	100.0
Flare and warp	Disk foreground	0.62	9.1	2.3
Flare and warp	Disk background	5.97	8.9	21.2
Flare and warp	Disk Total	3.25	18.0	23.5
Flare and warp	Disk > 15 kpc	13.60	1.3	7.1
Flare and warp	Disk > 11 kpc	10.04	3.4	13.7
Flare and warp	Bulge	2.33	82.0	76.4
Flare and warp	Total	2.50	100.0	100.0
SD, $v_{G,\phi} = 50$	Disk foreground	0.65	10.4	2.7
SD, $v_{G,\phi} = 50$	Disk background	5.15	7.4	15.4
SD, $v_{G,\phi} = 50$	Disk Total	2.52	17.7	18.2
SD, $v_{G,\phi} = 50$	Disk > 15 kpc	11.92	0.5	2.4
SD, $v_{G,\phi} = 50$	Disk > 11 kpc	8.81	2.3	8.1
SD, $v_{G,\phi} = 50$	Bulge	2.44	82.3	82.0
SD, $v_{G,\phi} = 50$	Total	2.45	100.0	100.0
SD, $v_{G,\phi} = 150$	Disk foreground	0.63	9.8	2.5
SD, $v_{G,\phi} = 150$	Disk background	5.43	8.0	17.6
SD, $v_{G,\phi} = 150$	Disk Total	2.78	17.8	20.2
SD, $v_{G,\phi} = 150$	Disk > 15 pc	12.05	0.8	3.9
SD, $v_{G,\phi} = 150$	Disk > 11 pc	9.09	2.9	10.8
SD, $v_{G,\phi} = 150$	Bulge	2.39	82.2	79.8
SD, $v_{G,\phi} = 150$	Total	2.46	100.0	100.0
SD, $v_{G,\phi} = 250$	Disk foreground	0.63	9.53	2.4
SD, $v_{G,\phi} = 250$	Disk background	5.47	8.27	18.5
SD, $v_{G,\phi} = 250$	Disk Total	2.87	17.8	20.9
SD, $v_{G,\phi} = 250$	Disk > 15 kpc	12.03	0.8	4.1
SD, $v_{G,\phi} = 250$	Disk > 11 kpc	9.12	2.75	10.2
SD, $v_{G,\phi} = 250$	Bulge	2.26	82.2	79.1
SD, $v_{G,\phi} = 250$	Total	2.45	100.0	100.0

Table 3. Model 2, $m_t = 20$

Model	Component	$10^6 \tau_i$	$100 f_i$	$10^8 \left(\frac{\tau_i f_i}{\tau} \right)$
Unperturbed	Disk foreground	0.62	13.8	3.6
Unperturbed	Disk background	5.24	12.3	27.5
Unperturbed	Disk Total	2.80	26.1	31.2
Unperturbed	Disk > 15 kpc	11.96	1.0	5.0
Unperturbed	Disk > 11 kpc	8.81	4.1	15.5
Unperturbed	Bulge	2.18	73.9	68.8
Unperturbed	Total	2.34	100.0	2.34
Flare and warp	Disk foreground	0.62	13.4	3.3
Flare and warp	Disk background	6.12	13.3	32.8
Flare and warp	Disk Total	3.34	26.9	36.1
Flare and warp	Disk > 15 kpc	13.89	2.11	11.8
Flare and warp	Disk > 11 kpc	10.28	5.2	21.6
Flare and warp	Bulge	2.18	73.1	63.9
Flare and warp	Total	2.49	100.0	100.0

Table 4. Model 2, $m_t = 22$

Model	Component	$10^6 \tau_i$	$100 f_i$	$10^8 \left(\frac{\tau_i f_i}{\tau} \right)$
Unperturbed	Disk foreground	0.63	10.5	2.7
Unperturbed	Disk background	5.43	10.5	22.9
Unperturbed	Disk Total	3.03	20.9	25.6
Unperturbed	Disk > 15 kpc	12.03	1.0	4.8
Unperturbed	Disk > 11 kpc	8.94	3.8	13.5
Unperturbed	Bulge	2.33	79.1	74.4
Unperturbed	Total	2.48	100.0	100.0
Flare and warp	Disk foreground	0.63	10.3	2.5
Flare and warp	Disk background	6.56	11.6	28.8
Flare and warp	Disk Total	3.77	22.0	31.3
Flare and warp	Disk > 15 kpc	14.06	2.3	12.0
Flare and warp	Disk > 11 kpc	10.67	5.0	20.2
Flare and warp	Bulge	2.33	78.0	68.6
Flare and warp	Total	2.65	100.0	100.0

Table 5. Model 1, $m_t = 20, b = -1^\circ, l = 1^\circ$

Model	Component	$10^6 \tau_i$	$100 f_i$	$10^8 \left(\frac{\tau_i f_i}{\tau} \right)$
Unperturbed	Disk foreground	1.0	12.2	2.8
Unperturbed	Disk background	9.37	16.2	35.2
Unperturbed	Disk Total	5.78	28.35	38.0
Unperturbed	Disk > 15 kpc	22.88	0.9	4.9
Unperturbed	Disk > 11 kpc	15.99	5.5	20.5
Unperturbed	Bulge	3.74	71.65	62.0
Unperturbed	Total	4.31	100.0	100.0

Table 6. Present velocity of Sagittarius dwarf

$v_{h,r}$	$v_{h,\phi}$	$v_{G,r}$	$v_{G,\phi}$
140.0	-220.2	167.6	0.0
140.0	-270.3	165.0	-50.0
140.0	-370.3	160.0	-150.0
140.0	-470.4	154.9	-250.0